VARIABLE ROTOR SPEED TRIM AND INTERACTIONAL AERODYNAMICS FOR QUADCOPTER UAS

Joon W. Lim
U.S. Army Combat Capabilities Development
Command Aviation & Missile Center
Ames Research Center
Moffett Field, California, U.S.A.

Austin D. Thai
Acoustics Engineer
Joby Aviation
Santa Cruz, California, U.S.A.

ABSTRACT

Variable rotor speed trim analysis for the SUI Endurance quadcopter has been successfully performed using the high-fidelity HPCMP CREATE™-AV Helios rotorcraft analysis and simulation framework. In forward flight, the 2DOF vehicle trim is applied using Helios/RCAS loose coupling, and the resulting Helios vehicle loads show marginal differences with the test data. The trimmed mean rotor speed and differential rotor speed are found moderately different from the test data. The 3DOF vehicle trim is explored to understand the effects of trim with fuselage pitch attitude as an additional trim variable. The effects of aerodynamic interactions are examined systematically using four CFD models: the isolated forward and aft rotor models, the model with all the rotors but without fuselage, and the full vehicle model. It is found that the forward rotor-to-aft rotor interaction is the most significant. In addition, the interaction on the forward rotors is found beneficial, whereas the interaction on the aft rotors degrades rotor thrust.

INTRODUCTION

Interest in unmanned aircraft system (UAS) and urban air mobility (UAM) has grown rapidly over the last decade. Their vertical lift capability showed great potential for surveillance missions, delivery systems, and transportation. As a part of Future Vertical Lift (FVL) program, the U.S. Army has initiated Future Tactical Unmanned Aircraft Systems (FTUAS). The FTUAS is the Army's premier Vertical Take-Off and Landing (VTOL) Unmanned Aircraft modernization effort and requires runway independence, point take-off and landing, and a rapidly deployable UAS capability to maintain its dominance in the field. As interest on the UAS/UAM configurations grows, research questions on their design, variable rotor speed trim and controls, and handling quality have consequently emerged.

UAS/UAM vehicles typically comprise multi-rotors with rotors operating at different RPMs (Refs. 1-4). The differential RPM between the front and rear rotors balances fuselage pitching moment while a sum of rotor thrusts contributes to vehicle lift and propulsive forces. Due to the existence of multiple rotors and airframe, strong aerodynamic interactions are unavoidable. Since the rotors operate typically at different RPMs, vehicle simulations are complicated and accordingly vehicle trim in simulation becomes challenging.

The Straight Up Imaging (SUI) Endurance quadcopter is an unmanned aerial vehicle, designed for aerial photography. The SUI Endurance uses four T-Motor carbon-fiber 15x5, two-bladed rotors, and the blade CAD geometry (Generation 1) was provided by SUI to NASA as part of a collaborative effort in NASA's Revolutionary Lift Vehicle. To better understand the performance characteristics of multirotor UAS configurations, NASA made significant efforts to generate wind tunnel test data. Carl Russell et al. performed wind tunnel tests at the U.S. Army 7- by 10-ft Wind Tunnel at NASA Ames Research Center (Refs. 1-2). The measurements were made for five different UAS configurations - 3DR SOLO, DJI Phantom 3, 3DR Iris+, Drone America x8 and SUI Endurance quadcopters – and included rotor forces and moments using a six-axis load cell and rotor operating RPMs for an isolated rotor and a fully integrated vehicle.

Zawodny and Pettingill conducted wind tunnel tests at the NASA Langley Low Speed Aeroacoustics Wind Tunnel (LSAWT) to obtain acoustic and load

Presented to the 49th European Rotorcraft Forum, Bückeburg, Germany, September 5-7, 2023.

measurements (Refs. 3, 4). The tests were focused on SUI Endurance quadcopter at the trim conditions in hover and at a freestream velocity of 15.5 m/s (M_∞ = 0.045). The vehicle pitch attitude was fixed at 0 degrees in hover and -10 degrees (fuselage nose down) in forward flight. This test data provides trimmed rotor RPMs for the SUI quadcopter at fixed fuselage pitch attitude.

There has been little effort made to conduct a trim analysis for quadcopter configurations. This work is built upon the prior work at AvMC on variable rotor speed trim for multi-rotor configurations. Pioneering work by Roget et al. (Ref. 5) developed the trim methodology using Helios coupled with RCAS and demonstrated its application using the UH-60A main rotor/tail rotor and DJI Phantom. Thai et al. (Refs. 6, 7) showed high-fidelity Helios predictions for the SUI endurance quadcopter, coupled with a multirotor trim solver based on the least squares approach. This paper extends the Thai et al. work by applying the Helios/RCAS coupled trim methodology (originally developed by Roget et al.) to this SUI Endurance configuration.

On the other hand, Diaz and Yoon (Ref. 8) conducted a detailed CFD study for various UAS multirotor vehicles with the prescribed trim condition given in Ref. 3. Although they did not quantify the effect of rotor/rotor and rotor/fuselage interactions, their study indicated the existence of strong interactions using CFD flow visualization.

Figure 1 displays the image of SUI Endurance quadcopter vehicle installed on Model Test Stand (MTS) in the LSAWT facility. The sequence and rotation direction of the rotors on the quadcopter are shown in Fig. 2. CW indicates clockwise rotor and CCW is a counterclockwise rotor. The property of T-Motor 15x5 rotor is provided in Table 1.

Table 1. T-Motor 15x5 rotor property.

Rotor radius	0.1905m (7.5in)
Blade mean chord	0.0283m (1.11in)
Nominal speed	3500 RPM
Reynolds number at 0.75R	93K
Hover tip Mach	0.2048
Rotor solidity	0.0829

COMPUTATIONAL METHODOLOGY

In the present study, two different fidelity analysis tools are used – low fidelity RCAS comprehensive analysis and high-fidelity Helios/RCAS coupled analysis.

Comprehensive Analysis, RCAS

The Rotorcraft Comprehensive Analysis System (RCAS) code is a comprehensive multi-disciplinary rotorcraft simulation code (Ref. 9). RCAS was jointly developed by the U.S. Army and Advanced Rotorcraft Technology, Inc. for predicting rotorcraft aerodynamic and structural loading, and the resulting performance, stability and vibration responses. It includes a library of primitive elements including nonlinear beams, rigid body mass, rigid bars, spring, damper, hinges and slides. Airloads are computed using various aerodynamic models. When coupled with Helios, RCAS computed airloads are replaced by the CFD provided data. In a loose coupling analysis, CFD periodic loads are computed over one rotor revolution and then used by RCAS to progressively update RCAS computed airloads by means of the delta-airload approach (Refs. 10, 11).

A typical vehicle trim analysis in rotorcraft is based on rotor periodic response, and the periodic rotor forces and moments that are averaged over one period are used for solving vehicle trim equations. Quadcopter in forward flight operates at various rotor speeds, which would result in different time periods for rotors. Thus, the various rotor periods require careful handling in collecting sampled rotor responses during the averaging process. Thus, the common time period of rotors in quadcopter should be defined as a least common multiplier of all four rotor periods, which can result in an impractical outcome - an infinitely large rotor common period and so requiring an impractically large computation time.

The ‘common period’ in RCAS (Ref. 12) is not an accurate representation of the common time period for variable rotor speeds in quadcopter. It is a single time period for all the rotors in quadcopter, which is a small integer multiple of the period of the reference rotor. The first rotor in the RCAS script is the reference rotor and typically labelled as Rotor1. In RCAS, a small arbitrary number (typically 4) is suggested for ‘common period’. A small number chosen for 'common period' reduces computation time in simulation to be manageable, but computational accuracy will be sacrificed. In the present study, 8 was chosen for 'common period', which means that the time spent for 8 cycles of the reference rotor is a time period for all the rotors in quadcopter.

Variable Rotor RPM Trim in RCAS

Quadcopters comprise multi-rotors with rotors operating at different RPMs. The differential RPMs between the front and rear rotors is a source to balancing fuselage pitch motion while a sum of rotor thrusts contribute to vehicle lift and propulsive forces.

Assuming symmetric rotor responses in the lateral direction, vehicle trim is achieved by satisfying the equilibrium equations in the airframe coordinate system (global frame) that is coincident with the fuselage orientation. The 3DOF vehicle trim requires to satisfy the following vehicle equations in the airframe coordinate system (global frame):

$$\sum(F_{z,i}) = 0 \qquad (1)$$
$$\sum(F_{x,i}) = 0$$
$$\sum(M_{y,i}) = 0$$

where *i* indicates contributing components from rotors and fuselage. Trim targets are set zero for the trim spring forces in the vertical (z) and longitudinal (x) axes and the trim spring moment in the pitch axis (y). Figure 3 indicates the sign convention of forces and moments of rotors and fuselage in the quadcopter. The 2DOF trim sets the trim spring vertical force and pitching moment equations to be zero with the trim variables of the mean rotor RPM and the differential rotor RPM.

Trim solves for the mean rotor speed of four rotors, differential RPM and vehicle pitch attitude. The differential RPM is defined as

$$\Delta RPM = (RPM_{FR} - RPM_{AR})/2 \qquad (2)$$

where FR and AR indicate forward and aft rotors respectfully. The mean rotor contributes to the total thrust from all the rotors reaching the target thrust. The differential RPM contributes to the vehicle pitching moment that is balanced with the pitching moments from all the components and those generated by rotor longitudinal forces (F_{xH}) multiplied by the distances from the fuselage center to the rotor hubs. The propulsive force generated by the rotor thrusts at a fuselage pitch attitude is balanced with the fuselage and rotor drag.

High-Fidelity Helios CFD Solver

The Helios CFD solver consists of two parts: a near-body solver that models and resolves the flow field near the solid bodies and an off-body solver that resolves the wake structures. The Unsteady Reynolds Averaged formulation of the Navier-Stokes equations (URANS) and their detached eddy simulation (DES) variants are usually employed to create an approach that balances efficiency and accuracy towards achieving practical simulations of rotorcraft systems. Helios supports a suite of near-body solvers (structured grid, unstructured grid or strand-based grid) that can operate in tandem within the same framework. The off-body solver in Helios uses a low dissipation high-order finite difference method that can transport and preserve wake structures and hence provide improved accuracy for aerodynamic interaction calculations. The detailed descriptions of various modules in Helios can be found in Ref. 13.

Helios mStrand (Ref. 14) is used for near-body solver in the present study. mStrand is a specialized strand grid solver that uses a vertex-centered finite-volume spatial discretization. The Reynolds-averaged Navier-Stokes (RANS) equations in a general moving coordinate system are solved. mStrand accommodates both quadrilateral and triangular surface elements and handles general prismatic meshes in the normal (strand) direction. The solver incorporates a second-order implementation of full Navier- Stokes for the viscous terms (no thin-layer approximation) and the option of using the Spalart-Allmaras or the Menter's k-ω SST turbulence models implemented with a first order discretization. More recently, the solver is also equipped with a first order discretization of several transition models including the Langtry-Menter (Ref. 15), Medida-Baeder (Ref. 16) and Coder's AFT (Ref. 17) models.

Figure 4 shows SUI Endurance rotors and fuselage grids with a cut through the off-body volume grids at the centerline of fuselage. Each rotor has two blades, and each blade has 199 points around the airfoil and 220 points along blade span with extending 0.4c in the strand direction using a default value of 51 points where c is the mean chord (= 0.0283m or 1.1in). The resulting near-body grid points are 17.9 million points for four rotors and 16.1 million points for fuselage, totaling 34.0 million grid points including fringe points.

It is worth noting that the near-body grids used in this study are the same near-body grids used in Ref. 7.

The off-body grids have 10 levels in grid refinement, extending 147R in each direction in order to avoid the effect of freestream boundaries. The fixed refinement box with a mesh size of 0.049c is defined in [-2.67R, 2.67R; -2.67R, 2.67R; -1.33R, 0.66R]. It is worth noting that Ref. 7 used a grid adaption for the off-body, whereas a fixed refinement is taken for this study. The finest mesh size of the off-body grids near the rotor and fuselage surface is about 0.049c. The off-body grid contains 314 million grid points including fringe points. In the present analysis, one degree was used for time step with a SA-DES turbulence model unless specified otherwise. The Helios/RCAS loose coupling was performed at every 360-time step (one rotor revolution). The computation time for the SUI full vehicle was taken 48.1 hours for 4320 time steps (12 rotor revolutions) on HPC Gaffney 960 cores.

DISCUSSION

Investigations into the aerodynamics of the SUI Endurance are presented for hover and forward flight. Single rotor performance is compared against the measured data for hover and full vehicle trim strategy and interactional aerodynamics are discussed for forward flight.

Hover Performance of an Isolated Rotor

RCAS simulations are performed using a prescribed wake analysis with the C81 airfoil tables generated using FUN3D CFD code that were provided by NASA. An adjustment of -1 degrees in blade aerodynamic twist is made in RCAS, which was shown in Ref. 18 that the adjustment produced more accurate simulation results.

The Helios results shown here were previously presented in Ref. 6. Figure 5a shows the comparison of Figure of Merit for the isolated rotor in hover. The test data from the U.S. Army 7- by 10-ft Wind Tunnel (7x10 WT) and the NASA Langley LSAWT are included. The Helios simulation was made using the SA-DES turbulence model. Although it shows a better trend than the RCAS result, it lacks 3-4 counts in FM. In order to see whether the transition model improves the FM results over the fully turbulent model, three transition models in Helios are considered: Langtry-Menter (Ref. 15), Medida-Baeder (Ref. 16) and Coder's AFT (Ref. 17) models. Figure 5b indicates that the transition models in Helios did not improve the FM results.

Table 2. Measured variable rotor speeds in forward flight at 15.5m/s for the SUI Endurance vehicle at the LSAWT facility. Fuselage pitch attitude was fixed at -10 degrees.

Thrust N	R1 RPM	R2 RPM	R3 RPM	R4 RPM
27N	3158	3132	3827	3827
36N	3641	3610	4425	4412
45N	3992	4047	4895	4937

Forward Flight Response with No Trim

The measured rotor speeds for the SUI Endurance vehicle are listed in Table 2, which was obtained from the LSAWT facility (Ref. 3). At 15.5m/s, the rotor speeds from all four rotors are provided at three vehicle thrust values: 27N, 36N and 45N, and the fuselage pitch attitude was fixed at -10 degrees. It is noted that positive pitch is defined fuselage pitch up. In an ideal situation, a quadcopter vehicle maintains symmetry side-by-side, but the actual rotor speed data shows small scatterings of rotor speeds between the side-by-side rotors. The scatterings of rotor speed can impact vehicle thrust by ±0.20N (0.75%), ±0.27N (0.78%) and ±0.55N (1.2%) for the target thrust of 27, 36 and 45N, respectively.

The Helios simulation with no trim was performed by prescribing the trim condition with the measured data. In Helios simulations, the forward rotor speed is prescribed with the measured Rotor 1 speed and the aft rotor speed is with the measured Rotor 3 speed.

Figure 6 compares the vehicle thrust, pitching moment and longitudinal force (F_x) computed using Helios against the test data (Ref. 3). Vehicle thrust and longitudinal force are defined positive up and aft respectively in the airframe coordinate system. Pitching moment is defined positive nose up. Some differences are observed between the test data and the Helios result. At a target thrust of 36N, the Helios thrust is higher by 2.7N (7.6% of the test data) than the test data (the measurement tolerance is 2.8%). The vehicle longitudinal force is overpredicted using Helios by 0.53N (6.6% of the test data), although it is still within the measurement tolerance (6.9%). It is worth noting that generating a longitudinal force of

0.53N requires a fuselage tilted by 0.8 degrees. Table 3 shows the uncertainty in the measurement of LSAWT data.

The Helios pitching moment in Fig. 6 is lower by 0.21Nm compared to the test data, and the cause of this difference is not well understood. To generate a pitching moment of -0.21Nm, the estimated increase in the forward rotor speed is about 45RPM (1.1% of the mean rotor speed). Contributions to vehicle pitching moment are further examined. Figure 7 shows the schematic image of the component forces and moments contributing to vehicle pitching moment. Table 4 shows the computed breakdown of contributions to vehicle pitching moment at the target thrust of 36N. Note that Vehicle M_y in Helios is a sum of all the moments from rotors and fuselage. It is found that vehicle pitching moment is contributed primarily by the pitching moments from the four rotors and the moments generated by the differential thrusts between the forward and aft rotors. The pitching moments generated by rotor forces are defined as:

(3) $$\sum \vec{\mathbf{X}}_{\mathbf{R}} \otimes \vec{\mathbf{F}}_{\mathbf{zH}} = -X_R \cdot \left[(F_{zH}^{R3} - F_{zH}^{R1}) + (F_{zH}^{R4} - F_{zH}^{R2}) \right]$$

(4) $$\sum \vec{\mathbf{Z}}_{\mathbf{R}} \otimes \vec{\mathbf{F}}_{\mathbf{xH}} = Z_R \cdot (F_{xH}^{R1} + F_{xH}^{R2} + F_{xH}^{R3} + F_{xH}^{R4})$$

Similar examination is made for vehicle drag. Figure 8 shows a schematic image of the component drag forces in the streamwise direction that are listed in Table 5. The rotor drag is computed from the rotor longitudinal force by projecting it to the streamwise direction. The fuselage drag is calculated by decomposing the fuselage longitudinal and vertical forces in the airframe coordinate system to the wind axis (streamwise direction). The combined fuselage and rotor drag force counteracts against the rotor propulsive force. The fuselage component forces and moments computed using Helios are provided in Table 6, which will be useful for the comprehensive code input.

Forward Flight Vehicle Trim

High-fidelity Helios results with no trim showed some differences in vehicle forces and moments from the

Table 3. The uncertainty in the measurement of LSAWT test data.

	F_x (N)	F_y (N)	F_z (N)	M_x (Nm)	M_y (Nm)	M_z (Nm)
Uncertainties (+/-)	0.5560	0.5560	1.0008	0.0282	0.0339	0.0452

Table 4. Computed breakdown of rotors and fuselage contributions to vehicle pitching moment using Helios with no trim at a target thrust of 36N and 15m/s. The rotor contribution is from all four rotors. X_R is 0.2565m (10.1in) and Z_R is 0.0305m (1.2in).

Helios					LSAWT
Rotors M_y	**Fuselage M_y**	$\sum \vec{\mathbf{X}}_{\mathbf{R}} \otimes \vec{\mathbf{F}}_{\mathbf{zH}}$	$\sum \vec{\mathbf{Z}}_{\mathbf{R}} \otimes \vec{\mathbf{F}}_{\mathbf{xH}}$	**Vehicle M_y**	**Vehicle M_y**
0.92	-0.13	-1.10	0.09	-0.23	-0.02

Table 5. Computed mean rotor and fuselage drag forces in the streamwise direction using Helios at 15m/s. Trim was prescribed with the test data.

Thrust	Fuselage drag	Drag from four rotors	Total drag
27N	5.43	2.33	7.76
36N	5.87	2.74	8.61
45N	6.32	3.09	9.41

Table 6. Computed fuselage aerodynamic loads using Helios at 15m/s. The dynamic pressure, q, is 142.56 Pa.

Thrust N	L/q m^2	D/q m^2	M/q m^3
27N	-0.00767	0.03734	-0.00082
36N	-0.00752	0.04048	-0.00091
45N	-0.00615	0.04393	-0.00097

test data. Observing these differences is not uncommon and the cause of the differences can be partly from modeling deficiency. Thus, trim is performed to reduce these differences.

First, a 2DOF vehicle trim is applied to satisfy the equilibrium of trim equations for the vehicle thrust and pitching moment in the airframe coordinate system. Trim variables are chosen as the mean rotor speed of four rotors and the differential rotor speed between the forward and aft rotors. Fuselage pitch attitude is fixed at -10 degrees.

Figure 9 shows trim iteration history of two trim variables - the mean rotor speed and differential rotor speed - at a target thrust of 27N, obtained using the 2DOF vehicle trim at 15m/s. In Helios/RCAS coupled analysis, simulation is made for a total of 4320 time steps (12 revs) with a time step size of 1 degree. Trim iteration is performed at every 360 time steps (1 rev), resulting in a total of 12 coupled trim iterations. Both the trim variables seem well converged within a tolerance of 2.5RPM.

Figure 10 compares the vehicle thrust, pitching moment and longitudinal force computed using a 2DOF vehicle trim against the test data at 15m/s. The Helios results shows marginal differences from the test data. At 36N, the differences of Helios result relative to the test data are: ΔFz = 0.68N (1.9% of the test data), ΔMy = -0.07Nm, ΔFx = 0.46N (5.7% of the test data). It is worth noting that all the forces are within the tolerance of the measurement and the 0.07Nm for the difference in pitching moment (ΔMy) is roughly equivalent to a change of the forward rotor speed by 15RPM (less than 0.4% of the measured mean rotor speed), which is trivial.

The trimmed rotor speed using a 2DOF vehicle trim is compared in Fig. 11. The predicted mean rotor speed is lower by 97 to 143 RPM (2.8 to 3.6% of the measured mean speed), and the predicted differential rotor speed is smaller by 57 to 60 RPM (1.3 to 1.6% of the measured mean speed) compared to the test data.

A 3DOF vehicle trim will be used for free flight trim. Using the Helios results with the 2DOF and 3DOF trim, Fig. 12 compares the computed vehicle thrust, vehicle pitching moment and vehicle longitudinal force, which shows marginal differences between the two trims.

Figure 13 compares the trimmed mean rotor speed and differential rotor speed between the 2DOF and 3DOF trims. It is found that the mean rotor speed from the 3DOF trim is higher by 81 to 161 RPM (2.3% to 4.0% of the mean rotor speed) and the differential rotor speed from the 3DOF trim is smaller by 20 to 52 RPM (0.5 to 1.5% of the mean rotor speed). Fuselage pitch is compared in Fig. 14 between the two trim cases. It is observed from the 3DOF trim result that a higher fuselage pitch (nose-down) attitude is required as vehicle thrust decreases, so as to generate sufficient propulsive force at a lower thrust. It is also found that fuselage drag increases as vehicle thrust rises due to an increase in rotor speed.

Interactional Aerodynamics in Forward Flight

Strong rotor/rotor and rotor/fuselage aerodynamic interactions are generally expected in quadcopter vehicles. In forward flight, tip vortex wakes generated from the forward rotors convect downstream towards aft rotors, resulting in strong rotor-to-rotor interactions. On the other hand, vortex wakes from the front part of fuselage travel downstream in the neighborhood of aft rotors, which generates another interaction between fuselage and rotors. Four CFD cases are chosen to understand the physics of these interactions for the SUI Endurance quadcopter (Fig. 15) as below:

- Case a: Isolated forward rotor
- Case b: Isolated aft rotor

Table 7. Comparison of forward and aft rotor thrusts for four CFD cases at the target thrust of 36N and 15m/s. The interaction effects are in the parenthesis.

	Forward rotor thrust (N)	Aft rotor thrust (N)
Case a, isolated fwd rotor	8.32 (--)	--
Case b, isolated aft rotor	--	12.08 (--)
Case c, all four rotors	8.57 (3.1%)*	10.98 (-9.1%)+
Case d, full vehicle	8.77 (5.5%)*	10.92 (-9.6%)+

*: relative to Case a

+: relative to Case b

- Case c: All four rotors
- Case d: Full vehicle

Flight condition was set with no trim by prescribing with the test condition at the target thrust 36N and a freestream velocity of 15m/s – the forward rotors operate at 3641RPM and the aft rotors at 4425 RPM with a fuselage pitch of -10 degrees.

Figure 16 shows the velocity flowfield and the non-dimensional normal force (M^2c_N) contour of isolated forward rotor (Case a), operating at 3641RPM. The flowfield was filtered by subtracting a freestream velocity of 15m/s. The leading blade is positioned at an azimuth of 126 degrees, and the cutting plane lies at y/R=0.89. The flowfield on the dvancing side appears complex. Multiple tip vortices pass by, and the velocity vectors behind the leading blade in the cutting plane (Fig. 16a) shows strong downwash. The contour of M^2c_N in Fig. 16b shows a hot spot near the blade tip in the second quadrant.

Figure 17 compares the M^2c_N contours of the isolated forward and aft rotors, operating at 3641RPM (Case a) and 4425RPM (Case b) respectively. It is indicated that the hot spot in the 2nd quadrant is much larger in Case b than Case a, which results from a higher rotor speed in Case b.

Figure 18 shows the Q iso-surface contours in the SUI vehicle and the M^2c_N contours of rotors. The streamlines were initiated in the upstream at a set of vertical points passing the hub center of Rotor 2. It is observed in Fig. 18a that the streamlines above the Rotor 2 rotor plane (clockwise rotation) swirl outward (blue arrow) when traveling towards Rotor 3, which may be due to the viscosity effects. The streamlines below the Rotor 2 rotor plane counteracts – the streamlines move inward when traveling tawards the Rotor 3 rotor plane (yellow arrow).

The interactional aerodynamics effects on rotor and fuselage are further examined. Rotor loads in Helios are obtained by integrating aerodynamic loads over the blade span and then summing the integrated airloads over two blades. Fuselage loads in Helios are computed by integrating airloads over the full airframe. Figure 19 compares the time history of rotor loads between the two isolated rotor cases – isolated forward rotor (Case a) and isolated aft rotor (Case b). Similarly, Figs. 20-21 show the time history of rotor and fuselage loads for the all four rotors (Case c) and full vehicle (Case d), respectively. Although they do not indicate directly the effects of interactions, these figures may be useful for the readers when the estimation of loads for rotors or fuselage is needed.

For direct comparison, the time histories of forward rotor are compared in Fig. 22 between the isolated forward rotor (Case a), all four rotors (Case c) and full vehicle (Case d). Similarly, the time histories of aft rotor are compared in Fig. 23 between the isolated aft rotor (Case b), all four rotors (Case c) and Ffull vehicle (Case d). The time history represents two rotor revolutions. Larger differences are observed for rotor thrust due to interactions, whereas rotor longitudinal force (Fx) and pitching moment (My) are less influenced. Table 7 shows a quantified comparison of the interaction effects for the four CFD cases. The quantities in parenthesis indicates a percentage change in thrust relative to the isolated rotor. Due to the interactions, the forward rotor gains thrust by 5.5% and the aft rotor loses it by 9.6% at the thrust of 36N. The 5.5% gain in the forward rotor thrust is partly due to the rotor-to-rotor interaction (3.1%) and fuselage (2.4%). The 9.6% loss in the aft rotor thrust is primarily due to the rotor-to-rotor interaction (-9.1%) with a mere 0.5% loss by the rotor/fuselage interaction. It is also found that the interaction on the forward rotors is beneficial, whereas the interaction on the aft rotors degrades rotor thrust.

CONCLUDING REMARKS

Variable rotor speed trim analysis has been successfully performed for the SUI Endurance quadcopter using the high-fidelity Helios/RCAS coupled analysis. The following are key findings from the present study:

1) A 2DOF vehicle trim at 15.5m/s was applied using Helios/RCAS loose coupling, and the predicted vehicle loads showed marginal differences from the test data. The predicted mean rotor speed was lower by 97 to 143 RPM (2.8 to 3.6% of the measured mean rotor speed) and the predicted differential rotor RPM was smaller by 57 to 60 RPM (1.3 to 1.6% of the measured mean rotor speed) compared to the test data.

2) The effects of aerodynamic interactions were examined. Due to the interactions, the forward rotor in a full vehicle gained thrust by 5.5% and the aft rotor lost thrust by 9.6% at a thrust of 36N. The forward rotor-to-aft rotor interaction was the most significant. The interaction on the forward rotors was beneficial, whereas the interaction on the aft rotors degraded rotor thrust.

ACKNOWLEDGEMENTS

The authors would like to acknowledge Carl R. Russell at NASA Ames Research Center and Martin K. Sekula at NASA Langley Research Center for providing CAMRAD II data of the SUI Endurance vehicle. The authors like to acknowledge Dr. Beatrice Roget, the U.S. Army DEVCOM AvMC D for providing help in setting the Helios input data and Dr. Hossein Saberi at Advanced Rotorcraft Technology, Inc. for providing help in setting the RCAS input data for quadcopter configuration.

REFERENCES

1. Russell, C., Jung, J., Willink, G., and Glasner, B., “Wind Tunnel and Hover Performance Test Results for Multicopter UAS Vehicles,” Proceedings of the AHS 72nd Annual Forum, West Palm Beach, FL, May 16-19, 2016.

2. Russell, C., Willink, G., Theodore, C., Jung, J., and Glasner, B., “Wind Tunnel and Hover Performance Test Results for Multicopper UAS Vehicles,” NASA TM-2018-219758, February 2018.

3. Zawodny, N. S., and Pettingill, N. A., “Acoustic Wind Tunnel Measurements of a Quadcopter in Hover and Forward Flight Conditions,” Proceedings of the Inter-Noise Impact of Noise Control Engineering Conference, Chicago, Illinois, August 2018.

4. Pettingill, N. A., and Zawodny, N. S., “Identification and Prediction of Broadband Noise for a Small Quadcopter,” Proceedings of the Vertical Flight Society 75th Annual Forum, Philadelphia, Pennsylvania, May 13–16, 2019.

5. Roget, B., Sitaraman, J., Blumenstein, R., Taheri, M., and Saberi, H., “Advanced Rotorcraft Aeromechanics Simulations using HPCMP CREATE™-AV Helios,” Proceedings of the VFS 75th Annual Forum, Philadelphia, PA, May 13-16, 2019.

6. Thai, A.D., "Development of high-fidelity computational methods for prediction of multirotor aerodynamics, aeroacoustics, and trim," Ph.D. Dissertation, Boston University, Boston, MA, 2022.

7. Thai, A. D., Roget, B., Sitaraman, J., and Grace, S. M., “Validation of Variable Rotor Speed Trim using Computational Fluid Dynamics,” to be published in *Journal of American Helicopter Society*, 2023.

8. Diaz, P. V., and Yoon, S., “High-Fidelity Computational Aerodynamics of Multi-Rotor Unmanned Aerial Vehicles,” Proceedings of the AIAA SciTech Forum 2018, Kissimmee, Florida.

9. Jain, R.K., Yeo, H., Ho, J.C. and Bhagwat, M., “An Assessment of RCAS Performance Prediction for Conventional and Advanced Rotor Configurations,” *Journal of American Helicopter Society*, Vol. 61, 2016.

10. Potsdam, M., Yeo, H. and Johnson, W., "Rotor railroads prediction using loose aerodynamic/structural coupling," *Journal of Aircraft*, 43(3), 2006, pp 732–742.

11. Lim, J. W., Nygaard, T. A., Strawn, R., and Potsdam, M., "Blade-Vortex Interaction Armloads Prediction Using Coupled Computational Fluid and Structural Dynamics," *Journal of the American Helicopter Society*, Vol. 52, (4), October 2007, pp. 318-328.

12. Anon., "RCAS User's Manual," Technical Report USAAMCOM/AFDD TR 02-A-006, U.S. Army Aviation and Missile Command, Moffett Field, CA, June 2014.

13. Wissink, A. M., Sitaraman, J., Jayaraman, B., Roget, B., Lakshminarayan, V. K., Potsdam, M. A., Jain, R., Bauer, A., and Strawn, R., "Recent advancements in the Helios rotorcraft simulation code," Proceedings of the 54th AIAA Aerospace Sciences Meeting, San Diego, CA, Jan. 4-8, 2016.

14. Lakshminarayan, V. K., Wissink, A. M., Jain, R. and Sitaraman, J., "Improvements to Automated Strand Meshing Capabilities for Rotary Wing Applications," Proceedings of the VFS International Transformative Vertical Flight 2020 Meeting, San Jose, CA, Jan. 21–23, 2020.

15. Langtry, R. B., and Menter, F. R., "Correlation-Based Transition Modeling for Unstructured Parallelized Computational Fluid Dynamics Codes," *AIAA Journal*, Vol. 47, No. 12, Dec. 2009, pp. 2894–2906.

16. Medina, S. and Baeder, J. D. "Application of the correlation-based $\gamma - R_{e\theta t}$ transition model to the Spalart-Allmaras turbulence model," AIAA-2011-3979, 20th AIAA Computational Fluid Dynamics Conference, Honolulu, HI, June 2011.

17. Coder, J. G., "Development of a CFD-compatible transition model based on linear stability theory," Ph.D. Dissertation, The Pennsylvania State University, State College, PA, 2014.

18. Russell, C., and Sekula, M. K., "Comprehensive Analysis Modeling of Small-Scale UAS Rotors," Proceedings of the AHS International 73rd Annual Forum, Fort Worth, Texas, USA, May 9-11, 2017.

Figure 1. SUI Endurance vehicle installed on Model Test Stand (MTS) in LSAWT (the images taken from Ref. 3).

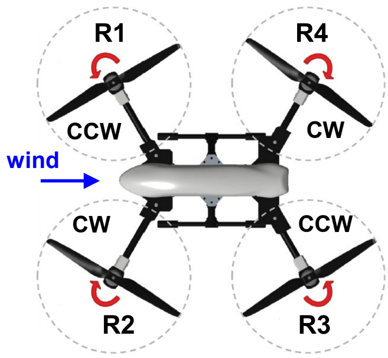

Figure 2. The image of SUI Endurance vehicle with rotor sequence Rotor sequence in the top view (the images taken from Ref. 3).

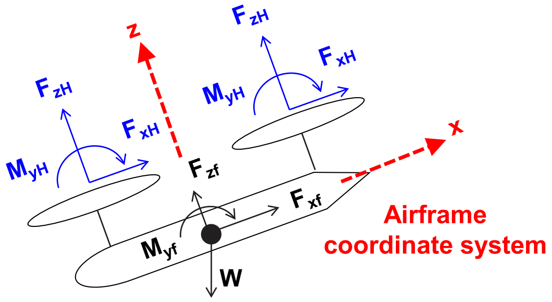

Figure 3. Sign convention of forces and moments of rotors and fuselage in the quadcopter airframe coordinate system.

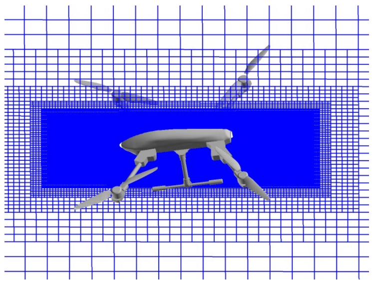

Figure 4. SUI Endurance rotors and fuselage grids with a cut through the off-body volume grids at the centerline of fuselage.

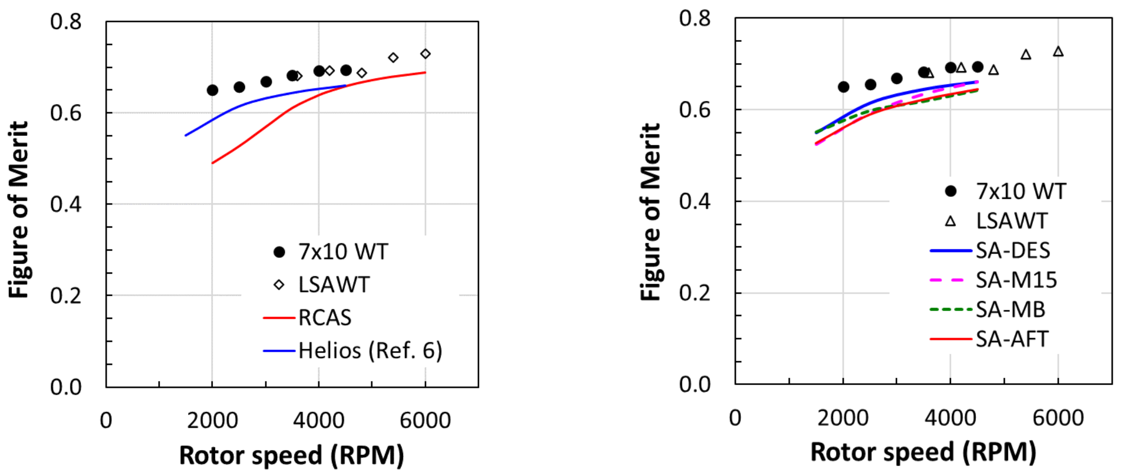

a) Figure of Merit computed using various codes

b) Figure of Merit computed using various transition models in Helios

Figure 5. Figure of Merit with rotor RPM for an isolated rotor in hover. The rotor is a two-bladed T-Motor 15x5 in the SUI Endurance vehicle. The Helios results were previously presented in Ref. 6.

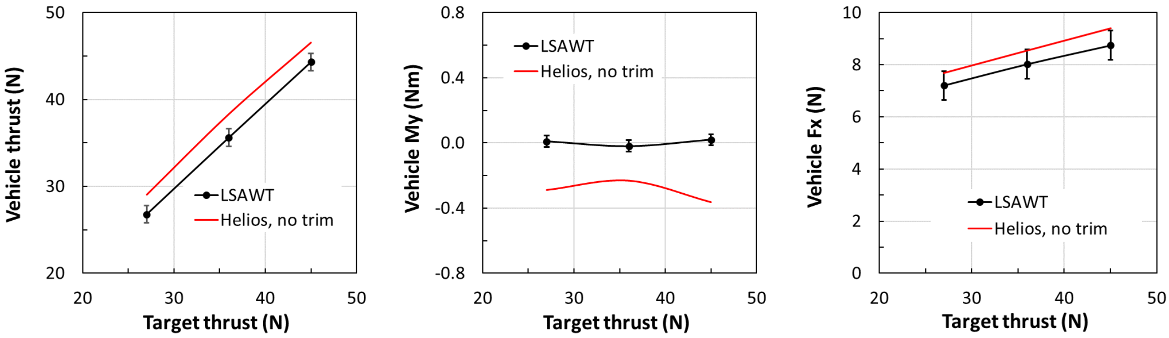

Figure 6. SUI vehicle loads in the airframe coordinate system, computed using Helios. The Helios simulation was performed with no trim. The trim condition was prescribed with the test data. Fuselage pitch attitude is fixed at -10 degrees. The error bars indicate measurement tolerances.

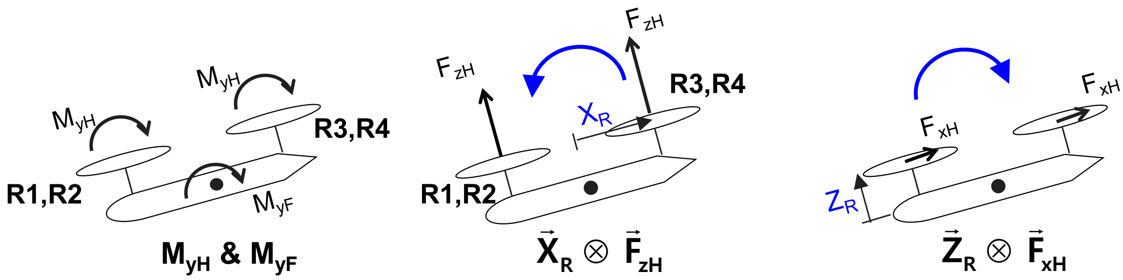

Figure 7. Schematic image of the component forces and moments contributing to the vehicle pitching moment in the airframe cooridinate system. The component forces include the rotor vertical (F_{zH}) and longitudinal (F_{xH}) forces.

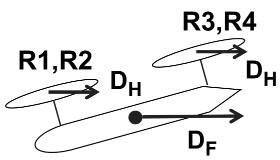

Figure 8. Schematic image of the component drag forces in the streamwise direction. The component drag forces include the rotor drag and fusle drag forces.

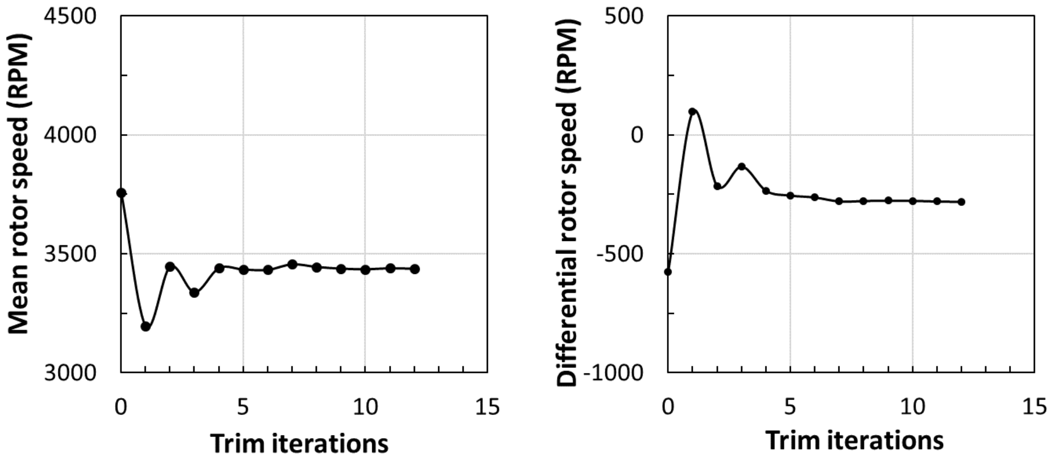

Figure 9. Trim iteration history of the mean rotor speed and differential rotor speed at a target thrust of 27N, obtained using the 2DOF vehicle trim at 15m/s. Fuselage pitch attitude is fixed at -10 degrees.

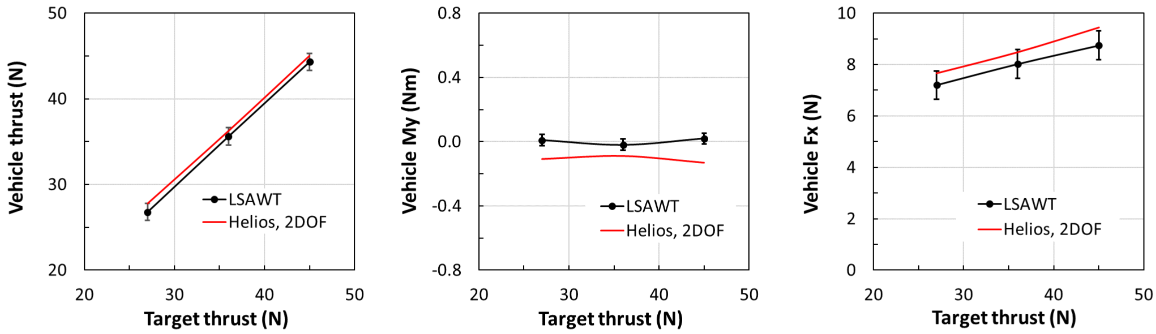

Figure 10. Trimmed vehicle loads in the airframe coordinate system at 15m/s using the 2DOF vehicle trim. Fuselage pitch attitude is fixed at -10 degrees. The error bars indicate measurement tolerances.

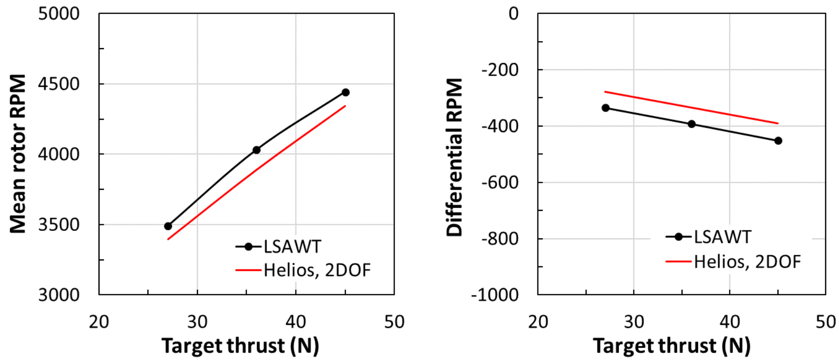

a) Mean rotor RPM **b) Differential rotor RPM**

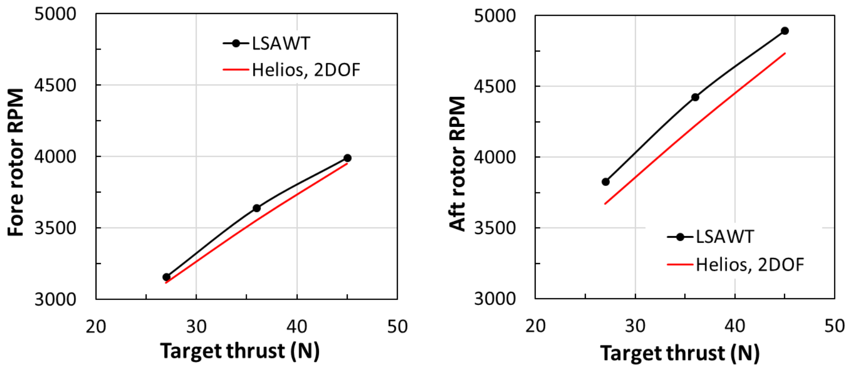

c) Forward rotor RPM **d) Aft rotor RPM**

Figure 11. Trimmed rotor speeds at 15m/s, computed using Helios with the 2DOF vehicle trim. Fuselage pitch attitude is fixed at -10 degrees.

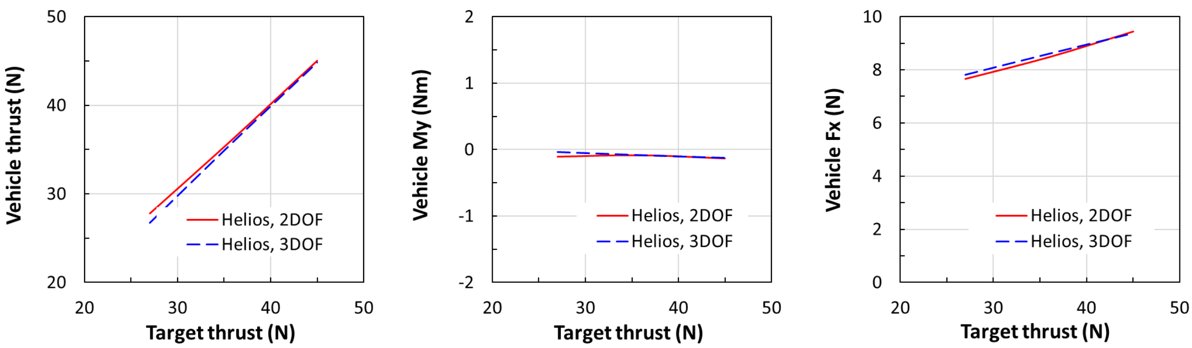

Figure 12. Trimmed vehicle loads in the airframe coordinate system at 15m/s, compared between the 2DOF and 3DOF trim.

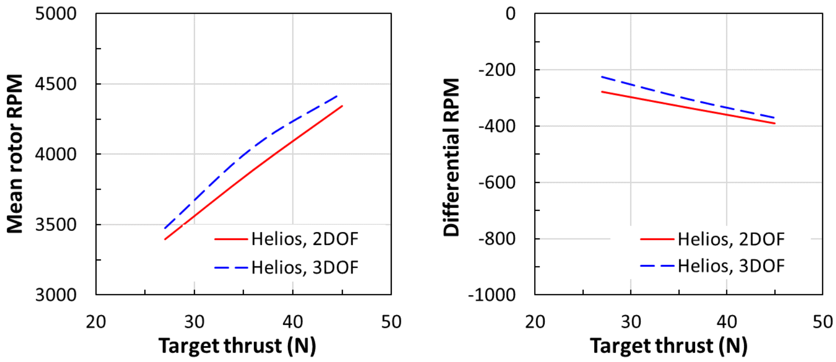

Figure 13. Trimmed mean rotor speed and differential rotor speed at 15m/s, compared between the 2DOF and 3DOF trim.

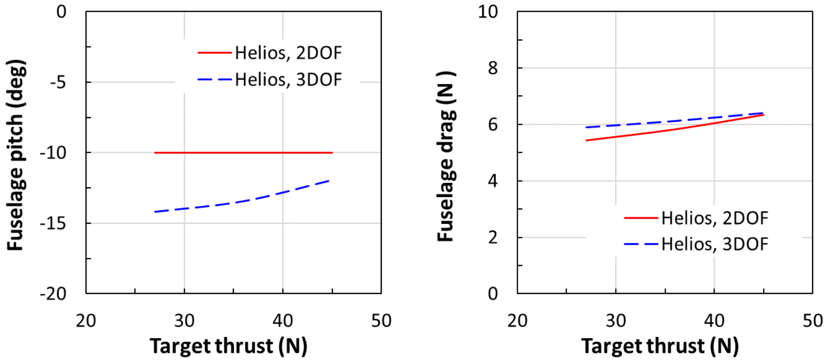

Figure 14. Trimmed fuselage pitch attitude and fusleage drag at 15m/s, compared between the 2DOF and 3DOF trim. Fuselage drag is in the streamwise direction.

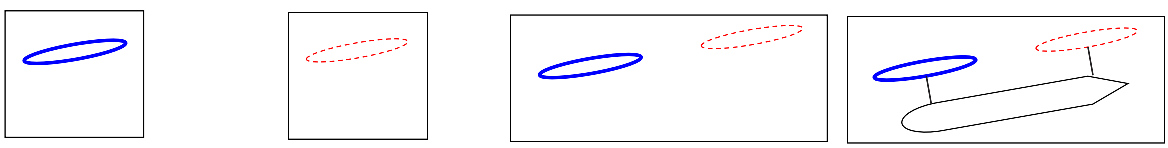

a) Isolated forward rotor at 3641RPM

b) Isolated aft rotor at 4425RPM

c) All four rotors

d) Full vehicle

Figure 15. Four CFD cases for the investigation of interactional aerodynamics at a vehicle thrust of 36N with a freestream velocity of 15m/s. Fuselage pitch attitude is fixed at -10 degrees. R1 = R2 = 3641RPM and R3 = R4 = 4425RPM.

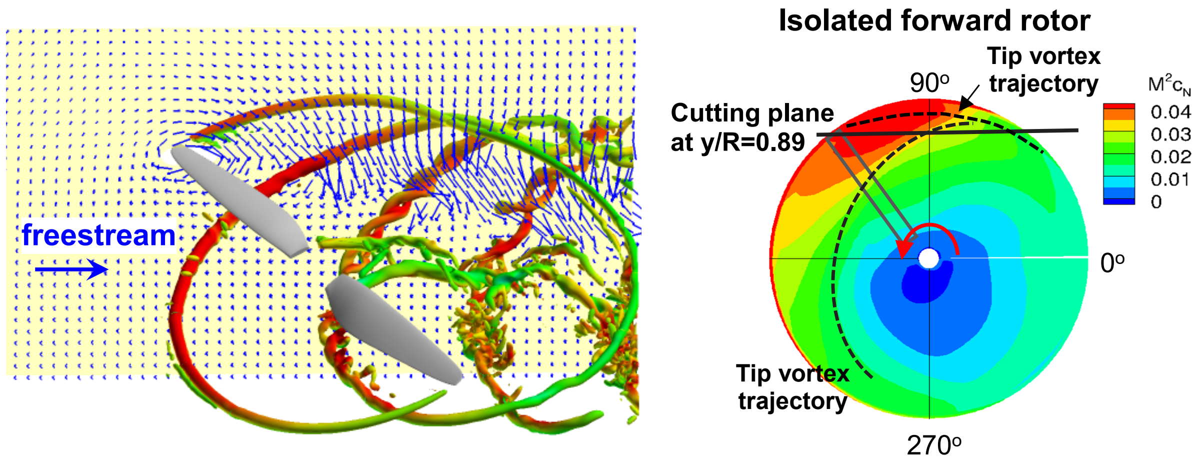

a) Flowfield in the cutting plane at y/R=0.89 b) M^2 c_N

Figure 16. Velocity flowfield and M^2c_N contour of the isolated forward rotor (Case a) at 3641RPM and 15m/s for a thrust of 36N. The flowfield was filtered by subtracting a freestream velocity of 15m/s. Fuselage pitch attitude is fixed at -10 degrees.

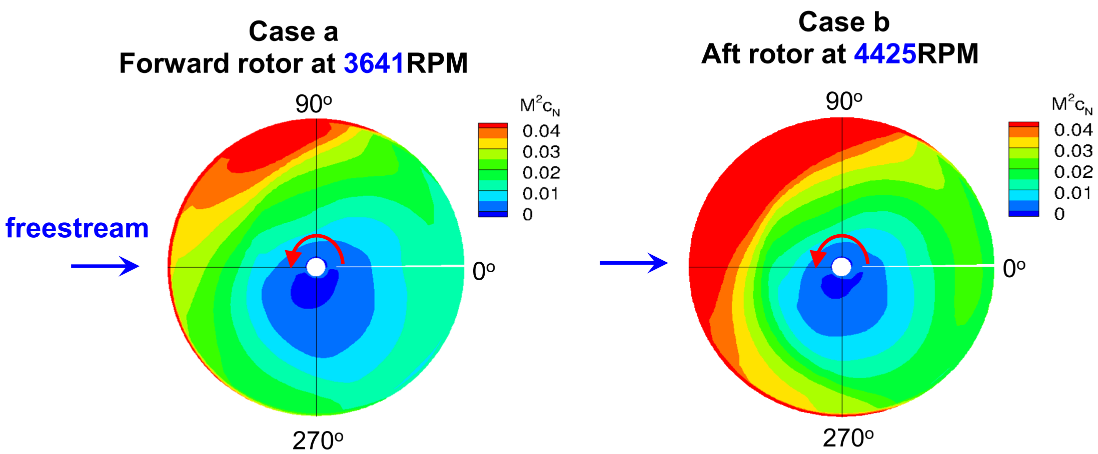

a) Isolated forward rotor (Case a) b) Isolated aft rotor (Case b)

Figure 17. M^2c_N contours of two isolated rotors (Case a and Case b) at 15m/s. Rotor shaft is fixed at -10 degrees.

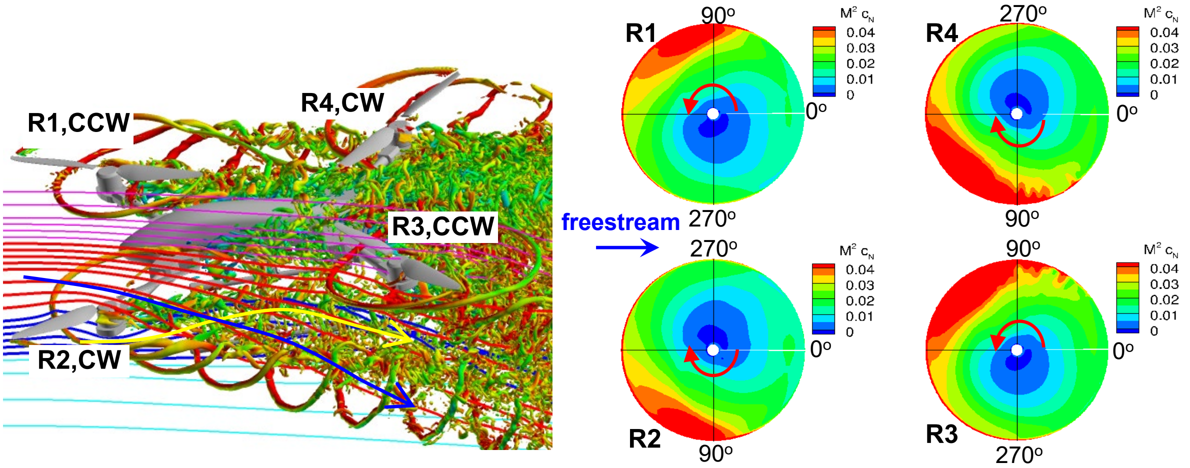

a) Q iso-surface

b) M^2 c_N contours of all the rotors

Figure 18. The Q iso-surface contours of the SUI vehicle (Case d) and the M^2c_N contours of rotors at 15m/s. Fuselage pitch attitude is fixed at -10 degrees. R1 and R2 at 3641RPM, and R3 and R4 at 4425RPM. Vehicle thrust is 36N. The streamlines are initiated in the upstream at a set of vertical points passing the hub center of Rotor 2.

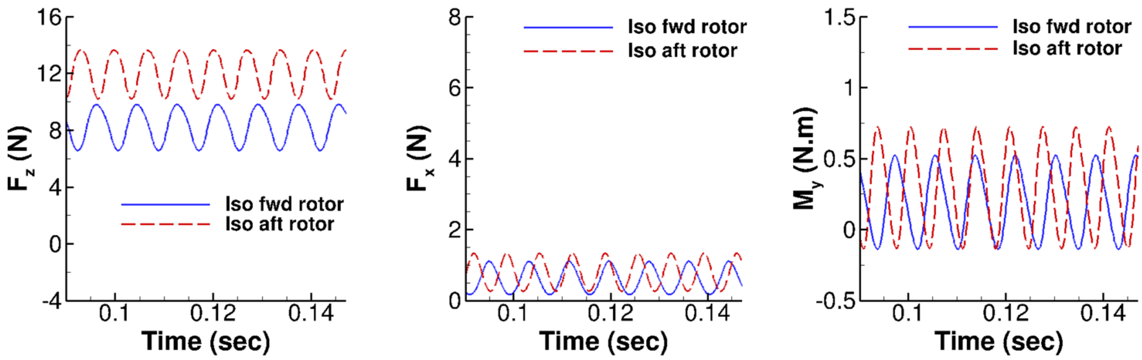

Figure 19. The comparison of the time history of rotor loads at 15m/s between the isolated forward rotor (Case a) and the isolated aft rotor (Case b). Rotor shaft angle is fixed at -10 degrees. Forward and aft rotor speeds are 3641RPM and 4425RPM, respectively.

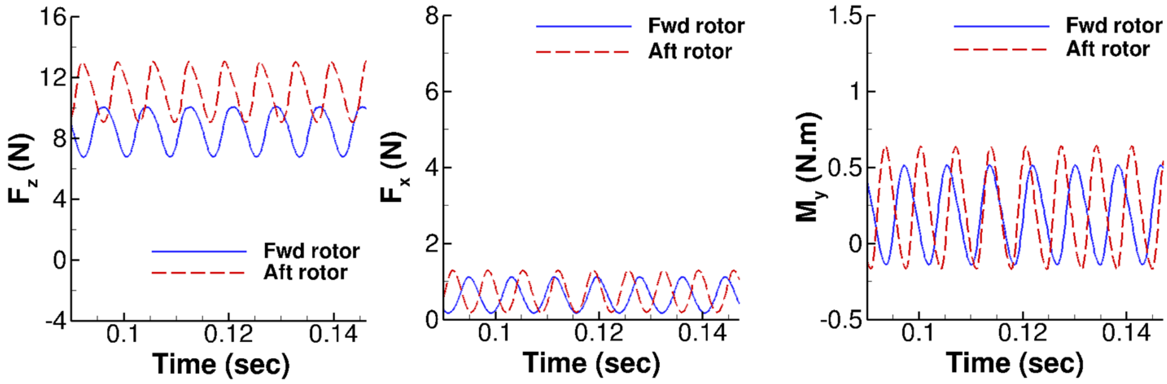

Figure 20. Time history of rotor loads at 15m/s for all four rotors (Case c). Rotor shaft angle is fixed at -10 degrees. Forward and aft rotor speeds are 3641RPM and 4425RPM, respectively.

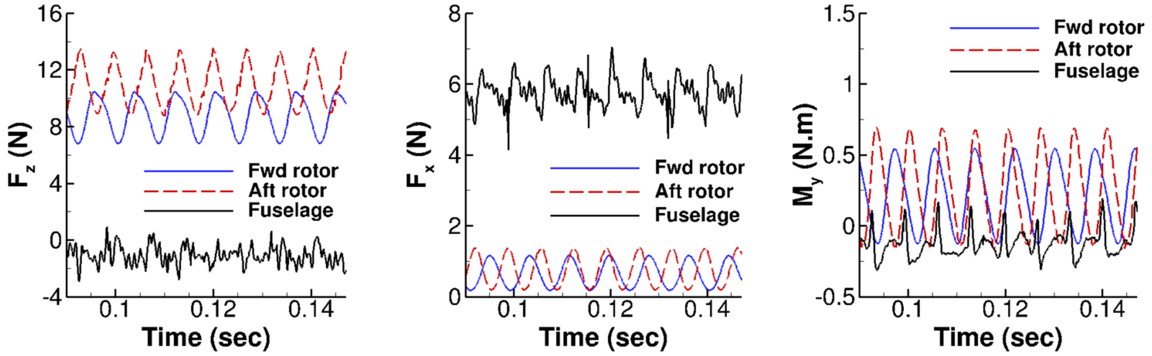

Figure 21. Time history of rotor loads at 15m/s for the full vehicle (Case d). Fuselage pitch attitude is fixed at -10 degrees. Forward and aft rotor speeds are 3641RPM and 4425RPM, respectively. Vehicle thrust is 36N.

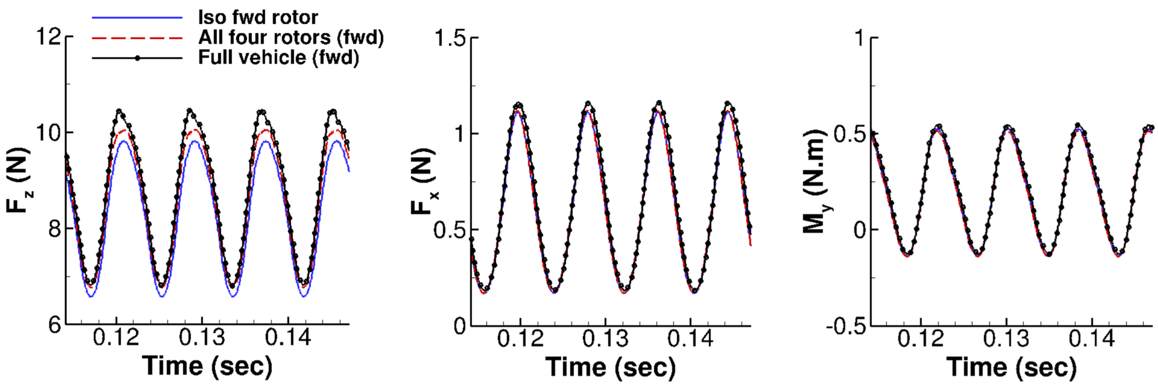

Figure 22. The comparison of the time history of forward rotor loads at 15m/s between the isolated forward rotor (Case a), all four rotors without the fuselage (Case c) and full vehicle (Case d). Fuselage pitch attitude is fixed at -10 degrees. Forward and aft rotor speeds are 3641RPM and 4425RPM, respectively. Vehicle thrust is 36N.

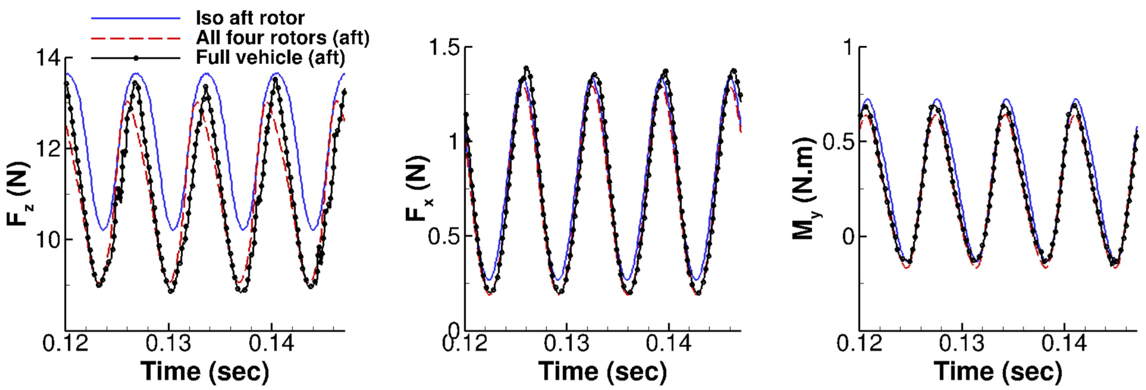

Figure 23. The comparison of the time history of aft rotor loads at 15m/s between the isolated aft rotor (Case b), all four rotors without the fuselage (Case c) and full vehicle (Case d). Fuselage pitch attitude is fixed at -10 degrees. Forward and aft rotor speeds are 3641RPM and 4425RPM, respectively. Vehicle thrust is 36N.